Phys. Status Solidi RRL 4, No. 7, 163–165 (2010) / DOI 10.1002/pssr.201004091

+++rapid research letters+++
www.pss-rapid.com

MOVPE growth and characterization of *a*-plane AlGaN over the entire composition range

Masihhur R. Laskar[*,1], **Tapas Ganguli**[2], **A. A. Rahman**[1], **A. P. Shah**[1], **M. R. Gokhale**[1], **and Arnab Bhattacharya**[1]

[1] Tata Institute of Fundamental Research, Homi Bhabha Road, Colaba, Mumbai 400005, India
[2] Raja Ramanna Center for Advanced Technology, Indore 425013, India

Received 20 March 2010, revised 9 May 2010, accepted 14 May 2010
Published online 21 May 2010

Keywords III–V semiconductors, AlGaN, MOCVD, X-ray diffraction

[*] Corresponding author: e-mail laskar@tifr.res.in, Phone: +91-22-22782261, Fax: +91-22-22804610

We report the metal organic vapor phase epitaxy (MOVPE) growth and characterization of non-polar $(11\bar{2}0)$ *a*-plane $Al_xGa_{1-x}N$ on $(1\bar{1}02)$ *r*-plane sapphire substrates over the entire composition range. $Al_xGa_{1-x}N$ samples with ~0.8 μm thick layers and with $x = 0, 0.18, 0.38, 0.46, 0.66$, and 1.0 have been grown on *r*-plane sapphire substrates. The layer quality can be improved by using a 3-stage AlN nucleation layer and appropriate V/III ratio switching following nucleation. All *a*-plane AlGaN epilayers show an anisotropic in-plane mosaicity, strongly influenced by Al incorporation and growth conditions. Careful lattice parameter measurements show anisotropic in-plane strain that results in an orthorhombic distortion of the hexagonal unit cell, making Al composition determination from X-ray diffraction difficult. In general lower Al incorporation is seen in *a*-plane epilayers compared to *c*-plane samples grown under the same conditions.

© 2010 WILEY-VCH Verlag GmbH & Co. KGaA, Weinheim

1 Introduction AlGaN, a wide bandgap semiconductor material, is very promising for UV-optoelectronics and high frequency devices. Nitride epilayers grown along the (0001) *c*-axis of the wurtzite crystal structure, suffer from undesirable spontaneous and piezoelectric polarization fields which impair device performance [1]. Thus, growth along "non polar" $(11\bar{2}0)$ *a*-plane and $(1\bar{1}00)$ *m*-plane ($\perp c$-axis) is being extensively pursued. Non-polar *a*-plane GaN layers have been grown on *r*-plane sapphire using different techniques [2–4], and there are a few reports of MOVPE grown *a*-plane AlGaN [5, 6]. From studies on *c*-plane AlGaN, it is known [7] that high quality epilayers are easier to grow on thick GaN buffers. However, deep UV LEDs ($\lambda \le 365$ nm), require AlGaN to be grown on transparent AlN buffer layers. Gas-phase reactions among precursors, low surface mobility of Al adatoms, and high sensitivity to V/III ratio and temperature make high quality AlGaN growth a challenge. In this Letter we present, to the best of our knowledge, the first synthesis of crack-free, *a*-plane AlGaN epilayers over the entire alloy composition via MOVPE.

2 Experiment AlGaN epilayers were grown via MOVPE in a $3 \times 2''$ closed-coupled showerhead reactor using trimethylgallium (TMGa), trimethylaluminium (TMAl) and ammonia (NH_3) precursors. For comparison between *a*-plane and *c*-plane AlGaN, both *r*-plane and *c*-plane sapphire were loaded in the same run. Improved layer quality was obtained using a 3-stage AlN nucleation layer – sequential deposition of 10 nm at 700 °C, 35 nm at 900 °C, and 35 nm at 1040 °C, at a V/III ratio of 1600. A set of 0.8 μm thick $Al_xGa_{1-x}N$ samples with $x_{gas} = 0, 0.2, 0.4, 0.5, 0.7, 1.0$ was grown at 1040 °C, V/III = 3000 and pressure 50 Torr. To change the alloy composition we varied the TMGa flow from 0 to 150 μmol/min at a fixed TMAl flow (28.5 μmol/min). Structural characterization of the epilayers was performed using a Philips X'PERT™ high resolution X-ray diffractometer with an asymmetric triple-axis analyzer and symmetric Ge(220) hybrid monochromator. Absorption measurements on backside polished samples were used to estimate the bandgap. The surface morphology was studied by optical interference contrast and atomic force microscopy.

WILEY InterScience® DISCOVER SOMETHING GREAT

© 2010 WILEY-VCH Verlag GmbH & Co. KGaA, Weinheim

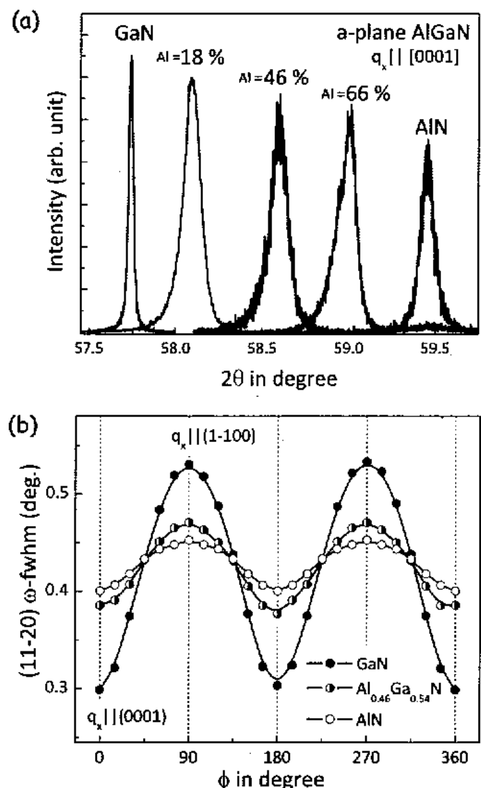

Figure 1 (online colour at: www.pss-rapid.com) (a) $\omega/2\theta$ X-ray scan of a series of *a*-plane AlGaN samples with x_{solid} = 0, 0.18, 0.46, 0.66, 1.0 at $q_x \parallel [0001]$. (b) $(11\bar{2}0)$ ω-fwhm as a function of in-plane rotation (ϕ) for three selected AlGaN samples showing the in-plane anisotropic mosaicity, which decreases with increasing Al content.

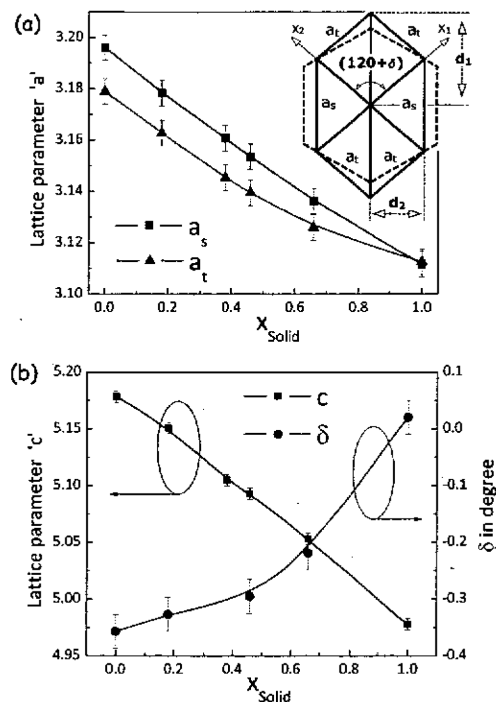

Figure 2 (online colour at: www.pss-rapid.com) (a) Variation in the sidewall (a_s) and top (a_t) lattice parameters as a function of Al incorporation x_{solid}. Inset: schematic diagram of the distorted hexagonal unit cell basal-plane. (b) Variation of *c*-axis lattice parameter and δ, the deviation from the 120° angle between the basal plane unit vectors as a function of x_{solid}. (Negative values of δ indicate angles <120°.)

3 Results Figure 1(a) shows $\omega/2\theta$ X-ray scans of the *a*-plane AlGaN samples over the entire composition range. The GaN profile is very sharp, with peak widths of AlGaN layers being relatively broad in comparison. Also the $(11\bar{2}0)$ ω-fwhm (along *c*-axis) increases with the increase in Al content. In case of AlGaN growth, Al adatoms have lesser surface mobility and larger sticking coefficient compared to the Ga atoms and are less likely to migrate to step edges and form smooth layers in a 2D growth mode [8]. The crystalline quality of the epilayers hence degrades on the addition of Al. The tendency towards island growth resulting in rougher layers is known from studies on *c*-plane AlGaN, the inherent anisotropy of the *a*-plane surface makes the situation more complex.

All the AlGaN epilayers show an in-plane anisotropy in the crystalline mosaicity, i.e., the $(11\bar{2}0)$ ω-fwhm varies periodically as a function of in-plane rotation (ϕ) as shown in Fig. 1(b). The $(11\bar{2}0)$ ω-fwhm value is maximum when the scattering plane is along the *m*-direction ($q_x \parallel [1\bar{1}00]$) and is minimum when the scattering plane lies along the *c*-direction ($q_x \parallel [0001]$). The $(11\bar{2}0)$ $\omega/2\theta$-fwhm and the (2θ) peak positions themselves do not change with the rotation ϕ. Figure 1(b) plots the $(11\bar{2}0)$ ω-fwhm for GaN, $Al_{0.46}Ga_{0.54}N$ and AlN. This anisotropy strongly depends on the Al content. GaN layers show the maximum anisotropy, which decreases on increasing Al incorporation. On *a*-plane oriented surfaces, the adatoms have larger incorporation probability and diffusion length along the [0001] direction [4]. This allows them a greater chance to find energetically favored positions and leads to a slightly faster growth rate and smaller ω-fwhm along the [0001] *c*-direction compared to $[1\bar{1}00]$ *m*-direction. It also results in a striated surface morphology as seen in optical interference contrast microscopy. The anisotropy reduces with the Al incorporation because of the smaller diffusion length of Al adatoms compared to Ga. The smaller diffusion length of Al also explains the increased roughness of AlGaN layers compared to GaN: the RMS roughness values for GaN and AlN measured from 2×2 μm^2 AFM scans are 4 nm and 18 nm, respectively. The microstructure and the anisotropy may also be influenced by the basal plane stacking fault density, the $(11\bar{2}0)$ reflection is however not sensitive to such defects [9].

For *c*-plane oriented films, an AlGaN epilayer on AlN is under uniform biaxial strain making the determination of lattice parameter and estimation of solid-phase Al incorporation (x_{solid}) relatively straightforward [10, 11]. However, for *a*-plane oriented films, the AlGaN epilayer on AlN buffer is under *anisotropic* biaxial strain as the lattice

© 2010 WILEY-VCH Verlag GmbH & Co. KGaA, Weinheim

mismatch and thermal expansion coefficients along the [0001] c-direction and [1$\bar{1}$00] m-direction are different. That results in an orthorhombic distortion of the hexagonal unit cell, making lattice parameter measurements and Al composition determination nontrivial [12, 13]. We have developed a detailed procedure for estimating the lattice parameters of orthorhombic distorted structures and an expression for estimating x_{solid} for such ternary alloys [14]. A schematic diagram of the distorted hexagonal unit cell is shown in the inset of Fig. 2(a). In this case the inter-planer distances can be described by $1/d_{hkl}^2 = (h^2+k^2-2hk\cos\gamma)/(a\sin\gamma)^2 + l^2/c^2$, where $\gamma = 120° + \delta$ is the angle between the x_1 and x_2 axes, $\alpha = \beta = 90°$ [15]. Unlike a regular hexagon, we need two different lattice parameters a_s (sidewall) and a_t (top) for a complete description of the distorted basal plane. Figure 2 shows that the lattice parameters a_s, a_t, and c decrease whereas δ increases as a function of x_{solid}. As x_{solid} increases, the anisotropic biaxial strain between AlGaN layer and AlN buffer decreases, hence the value of $|a_s - a_t|$ and δ decrease monotonically. Using the lattice parameters, and incorporating the effects of strain, for small distortions ($\delta < 1°$), x_{solid} can be expressed as

$$x_{solid} \approx \frac{(c_G - c)d_1d_2 + \gamma_1(d_{1G} - d_1)cd_2 + \gamma_2(d_{2G} - d_2)cd_1}{(c_G - c_A)d_1d_2 + \gamma_1(d_{1G} - d_{1A})cd_2 + \gamma_2(d_{2G} - d_{2A})cd_1},$$

where $d_1 = 2d_{11\bar{2}0} = (2a\sin\gamma)/\sqrt{2(1-\cos\gamma)}$ and $d_2 = d_{1\bar{1}00} = (a\sin\gamma)/\sqrt{2(1+\cos\gamma)}$; a, c and γ are the lattice parameters of the distorted AlGaN epilayer; subscripts G and A denote GaN and AlN, respectively (i.e., c_G is the c-lattice parameter of GaN); $\gamma_1 = C_{11}/C_{13}$ and $\gamma_2 = C_{12}/C_{13}$, where C_{11}, C_{12}, C_{13} are the elastic stiffness constants.

To verify the accuracy in x_{solid} estimated from the lattice parameters, we have also used optical transmission data to estimate x_{solid}. Figure 3 (inset) shows the transmission cut-off of a-plane AlGaN epilayers of different compositions. The bandgap of AlGaN can be expressed as [10] $E_g^{AlGaN} = xE_g^{AlN} + (1-x)E_g^{GaN} + bx(1-x)$, where E_g^{GaN}, E_g^{AlN}, and E_g^{AlGaN} are the bandgaps of GaN, AlN and AlGaN, respectively. We use $b = 1 \pm 0.2$ eV, a value determined from our c-plane AlGaN samples and similar to that reported in literature [16], to estimate x_{solid} for the a-plane AlGaN. The effect of anisotropic biaxial strain on the bandgap is estimated from data available for c-plane GaN [17]; for the strains measured in our samples the change in bandgap is $E_g \approx 20$ meV, corresponding to a change in x_{solid} of about $\pm 1\%$. The values of x_{solid} estimated from the X-ray data via strain-tensor calculations and from optical transmission are within 2%, providing a reasonable error-bound on the Al content.

Figure 3 shows the variation of x_{solid} as a function of gas-phase Al concentration (x_{gas}). A near-linear behavior indicates minimal gas phase pre-reactions. For the same x_{gas}, the Al incorporation is slightly larger in c-plane films than in a-plane films. For mass transport limited growth, x_{solid} depends on the relative fluxes of Al and Ga atoms diffusing to the surface, which in the same growth run, are the same for the two surfaces. The lower solid phase Al incorporation for a-plane AlGaN is probably due to differences in the relative sticking coefficients and incorporation probabilities for the two surfaces, further influenced by the a-plane surface anisotropy.

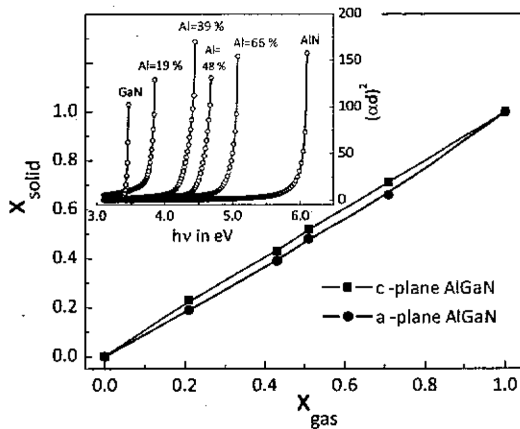

Figure 3 (online colour at: www.pss-rapid.com) Variation of Al incorporation in the epilayer, x_{solid}, as a function of x_{gas} = TMAl/[TMAl + TMGa] ratio in the gas phase, for c- and a-plane samples. Inset: Square of the absorption coefficient-thickness product as a function of photon energy for the a-plane AlGaN samples. The Al content determined from the absorption cut off values – x_{solid} = 0, 0.19, 0.39, 0.48, 0.66, 1.0 – is within 2% of that determined from analysis of lattice parameters.

In conclusion we report the synthesis and characterization of a-plane AlGaN epitaxial layers across the entire alloy composition range. The layers are mosaic and anisotropic due to an orthorhombic distortion in the hexagonal unit cell resulting from anisotropic biaxial strain. For such systems, we estimate solid phase Al incorporation using lattice parameters within reasonable accuracy. The demonstration of such AlGaN layers would help to develop nonpolar nitride based UV devices.

References

[1] T. Paskova, Phys. Status Solidi B **245**, 1011 (2010).
[2] T. S. Ko et al., J. Cryst. Growth **300**, 308 (2007).
[3] J. L. Hollander et al., App. Phys. Lett. **92**, 101104 (2008).
[4] H. Wang et al., Appl. Phys. Lett. **84**, 499 (2004).
[5] H. M. Huang et al., J. Cryst. Growth **312**, 869 (2010).
[6] T. J. Badcock et al., J. Appl. Phys. **105**, 123112 (2009).
[7] C. McAleese et al., J. Cryst. Growth **272**, 475 (2004).
[8] M. A. Khan et al., Jpn. J. Appl. Phys. **44**, 7191 (2005).
[9] M. A. Moram et al., J. Appl. Phys. **105**, 113501 (2009).
[10] H. Angerer et al., Appl. Phys. Lett. **71**, 1504 (1997).
[11] M. A. Moram et al., Rep. Prog. Phys. **72**, 036502 (2009).
[12] C. Roder et al., J. Appl. Phys. **100**, 103511 (2006).
[13] V. Darakchieva et al., Phys. Rev. B **75**, 195217 (2007).
[14] http://www.tifr.res.in/~arnab/latticeprocedure.pdf
[15] B. D. Cullity, Elements of X-ray Diffraction (Addison-Wesley, Reading, MA, 1978), p. 30 and Appendix 1.
[16] Y. Koide et al., J. Appl. Phys. **61**, 4540 (1987).
[17] A. Shikanai et al., J. Appl. Phys. **81**, 417 (1997).

© 2010 WILEY-VCH Verlag GmbH & Co. KGaA, Weinheim